Autonomous Single-Phase Grid-Connected Photovoltaic System

Ahmed A. A. Hafez

Electrical Engineering Department, Faculty of Engineering, University of Assiut
Assiut, PO 71516 Egypt

Abstract **- This paper proposes a simple and efficient controller for single-phase grid-connected photovoltaic system. The controller maintains the system operation at maximum power point at different levels of solar irradiance/temperature. A detailed design of the controller and the DC capacitor were carried out. An average-value model was developed to facilitate the design of the controller and to study the system performance under different operation conditions. The results were validated by rigorous simulation.**

Index Terms – Photovoltaic generator, Average-value model, Maximum power point.

I. INTRODUCTION

The Photovoltaic (PV) systems are the key technology for providing sustainable, eco-friendly and reliable electrical power source [1-2]. The PV systems, basically are classified into stand-alone, grid-connected or hybrid systems.

In small residential PV grid-connected systems, [3] the approach of single DC string, single DC-AC inverter has the advantages of simplicity and reduced cost. In this scheme, the PV panels are series connected to create a high voltage and low current DC source. A single-phase inverter interfaces this DC source into the residential switchboard.

The grid-connected PV systems generally shape the grid current to follow a predetermined sinusoidal reference using hysteresis-band current controller [4-10], which has the advantages of inherent peak current limiting and fast dynamic performance. However, the hysteresis controller employs variable switching frequency. The value of the switching frequency varies from maximum value near zero cross to a minimal near the peak of the waveform. Such modulation strategy produces random and unpredictable harmonics, which are not only pulse-width modulated but frequency-modulated as well. That pattern has the disadvantages of stressing the power switching devices, and producing undefined frequency spectrum, which complicates the design of the filters [4-10].

For best utilization, PV systems have to operate at their Maximum Power Point (MPP). However, the MPP varies with the insolation, temperature and other ageing effects. Numerous MPP Trackers (MPPTs) were reported in the literature [11-14]. The methods vary in complexity, cost, sensors required, convergence speed, range of effectiveness, availability, and implementation hardware. In general, the MPPT continuously adjusts the solar array terminal voltage/current, such that the array delivers maximum power at different climatological and environmental conditions.

The Incremental Conductance (IncCond) is a MPPT that has good convergence speed, moderate implementation complexity and precise tracking for MPP. The IncCond was developed based on the fact that the slope of PV module power-voltage curve is zero at MPP, positive right MPP and negative on the left. Since, the slope of power-voltage curve of a PV generator could be expressed by [11,13,14],

$$\frac{dP_{pv}}{dV_{pv}} = I_{pv} + V_{pv}\frac{dI_{pv}}{dV_{pv}} \tag{1}$$

where I_{pv}, V_{pv} and P_{pv} are current, voltage and power of PV module. Thus the relation between the incremental and instantaneous conductance is given by,

$$\begin{aligned} &\frac{\Delta I_{pv}}{\Delta V_{pv}} \succ \quad \text{MPP} \\ &\frac{\Delta I_{pv}}{\Delta V_{pv}} = -\frac{I_{pv}}{V_{pv}}, \text{ at MPP} \\ &\frac{\Delta I_{pv}}{\Delta V_{pv}} \prec \quad \text{t MPP} \end{aligned} \tag{2}$$

MPP is tracked by continuously comparing the incremental and instantaneous conductance and incrementing/decrementing the PV voltage/current.

This paper proposes a simple and efficient single-phase grid-connected PV system. The IncCond is used to extract the reference current then a simple proportional-integral (PI) controller is proposed to ensure the system operation at MPP irrespective of atmospheric conditions. An average model was developed to facilitate the design of the controller and to investigate the system performance under different operation conditions. A detailed design of the DC-link capacitor and the controller were carried out. The proposed system could be used for residential PV systems particularly in rural areas, due to the reduced cost and simplicity.

II. PROPOSED SYSTEM

The proposed system consists of PV generator, single-phase H-bridge inverter, output filter, PI controller and grid as shown in Fig. 1. The current at maximum power point I_{pvmax}, reference current I_{ref}, is extracted through Incremental Conductance method and compared with the PV generator current I_g. The error signal drives the compensator to generate

the angle of the inverter output voltage δ with respect to supply voltage.

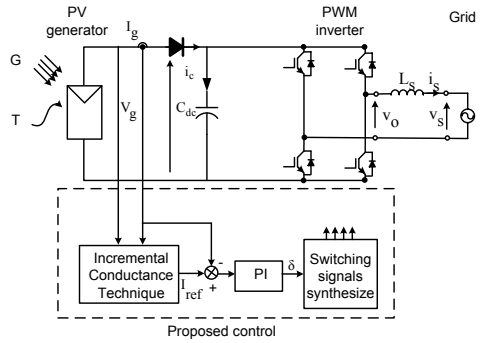

Fig. 1 Single-phase grid-connected PV system

Different models are proposed for depicting the characteristics of a PV cell; these models vary in accuracy and complexity. However, an moderate complexity model is used in the system under concern, Fig. 2.

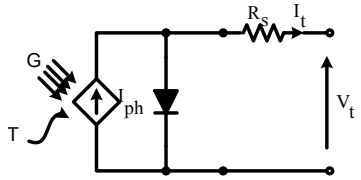

Fig. 2. Equivalent circuit of PV cell

The PV cell is modelled as a solar irradiation and temperature dependent current source I_{ph} in parallel with diode. This combination is in series with a series resistance R_s [15,16]. The proposed model of the PV has the merits of accuracy, robustness and simplicity. The relation between the terminal current I_t and voltage V_t of a PV cell is expressed by,

$$I_t = I_{ph} - I_o \left(e^{\frac{V_t + IR_s}{V_{th}}} - 1 \right) \quad (3)$$

where I_o and I_{ph} are saturation and generated currents . $V_{th} = nN_s kT/q$ is thermal voltage of the module; n, N_s , K, T and q are ideality factor, number of cells in series, Boltz's man constant and electron charge respectively.

PV cell basically has an output voltage less than 1 V, thus these cells have to be grouped in series/parallel arrangements to generate reasonable voltage/power level. These are defined as PV modules. The PV modules are further grouped in series-parallel arrangement to form array, which is defined in the proposed work as PV generator. Each PV generator consists of 30 Kyocera KC 200GT modules, and occupies the area of approximately 30 m^2 . The parameters of Kyocera KC 200GT module are given in Table 1, [15].

TABLE I
PARAMETERS OF KYOCERA KC200GT [15]

Temperature(°C)	25
Open circuit voltage (V)	32.9
Short circuit current (A)	8.21
Voltage at maximum power (V)	26.3
Current at maximum power (A)	7.61
Maximum power (W)	200

The relation between the PV generator terminal voltage V_g and current I_g could be expressed by an equation similarly to (3), however it more meaningful to express the PV generator current in terms of the voltage, short-circuit current I_{sc} and open-circuit voltage V_{oc} of the module, as these data are commonly supplied by the manufacturers at standard conditions, Table 1.

$$I_g = M_{ss} I_{sc} \left(1 - \exp\left(\frac{V_g - N_{ss} V_{oc} + \frac{N_{ss} I_g R_s}{M_{ss}}}{N_{ss} V_{th}} \right) \right) \quad (4)$$

where M_{ss} and N_{ss} are numbers of shunt and series connected modules respectively. The current I_g and the power P_g of the PV generator as a function of its voltage V_g calculated at 25°C and different radiation levels are given in Figs. 3.

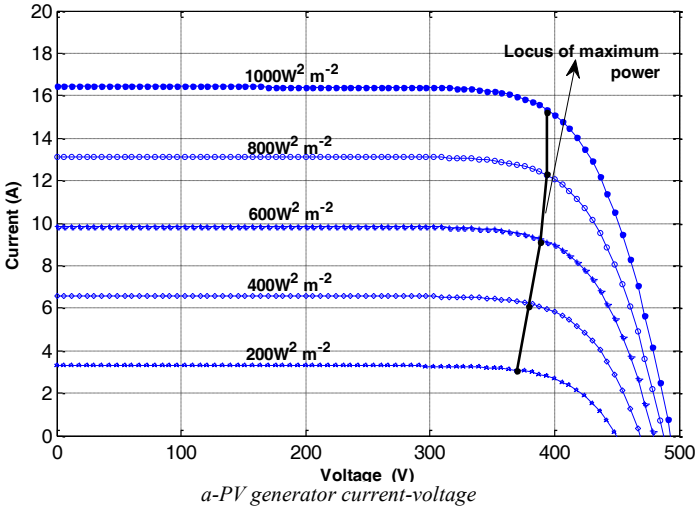

a-PV generator current-voltage

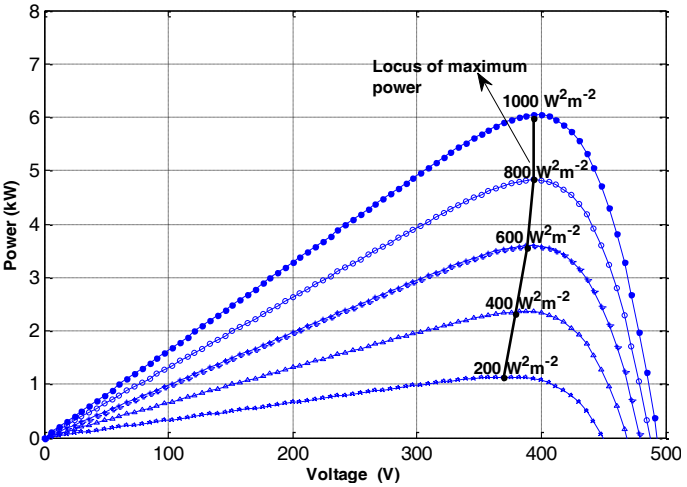

b-PV generator power-voltage

Fig. 3 PV generator current I_g (a) and power P_g (b) versus voltage at different solar irradiance levels and 25°C

Fig. 3 reveals that the PV generator current is linearly proportionated with the solar irradiance and hence the power. Moreover, the voltage at MPP is less dependent on the solar irradiance, since the voltage V_{MPP} drops by less 8% for 80% variation in the irradiation [14].

The proposed controller in Fig. 1 will continuously adjust the generator output current to track the reference. The reference current I_{ref} represents the PV generator current at maximum power point. The relation between the current I_{ref} and phase shift δ, where δ is the angle between the grid voltage v_S and the inverter output voltage v_O, could be derived by assuming that the system is lossless; therefore the power transferred to the grid equals the maximum generator output power P_{gmax}.

$$P_{gmax} = I_{ref} V_g = \frac{|V_{o1}||V_S|}{4\pi f L_S} \sin(\delta) \tag{5}$$

The modulation strategy ensures that the amplitude of inverter fundamental output voltage $|V_{o1}|$ equals to the PV generator voltage V_g, $|V_{o1}| = V_g$; thus according to (5) the angle δ and hence grid power are controlled by the reference current I_{ref}. Moreover, since I_{ref} represents the PV generator current at maximum power point; therefore, the controller forces the system to always operate at MPP.

III. AVERAGE-VALUE MODEL

To facilitate the design of inverter and the controller, an average-value model of the system is derived. The average-value model of the single-phase PWM inverter is obtained by averaging the switching states of the inverter over a switching cycle, then averaging the resultant over the fundamental frequency cycle. Accordingly the inverter model can be expressed mathematically by,

$$L_S \frac{di_S}{dt} = |V_g| \sin(\omega t+\delta) - |V_S| \sin(\omega t) - i_S R_S \tag{6}$$

$$C_{dc} \frac{dV_g}{dt} = I_g - i_S \sin(\omega t+\delta) \tag{7}$$

These equations are represented in Fig. 4 by the voltage source v_{o1} in the AC side, and the current source I_o in the DC side.

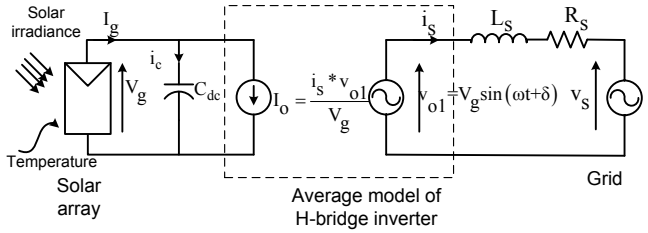

Fig. 4 Average model of single-phase grid-connected PV system

The input current of a single-phase inverter I_o contains significant 2nd harmonic ripple component. This is shown by equating the instantaneous inverter input and output powers and assuming sinusoidal inverter output voltage and current.

$$I_O = i_S \sin(\omega t+\delta) = \frac{|I_S|}{2}\left(\cos(\delta) - \cos(2\omega t+\delta)\right) \tag{8}$$

The low frequency current ripple component has to flow through the DC capacitor C_{dc}, otherwise it circulates in the PV generator producing significant power loss. Neglecting the capacitor parasitic resistance and switching ripples, the capacitor voltage ripple V_{gpp} is obtained by integrating the component in (8) at twice the grid frequency.

$$V_{gpp} = \frac{1}{C_{dc}} \int \frac{|I_S|}{2} \cos\left(2\omega t+\delta-\frac{\pi}{2}\right) dt = \frac{|I_S|}{4C_{dc}\omega} \sin\left(2\omega t+\delta-\frac{\pi}{2}\right) \tag{9}$$

The value of DC filter capacitor C_{dc} can be obtained by,

$$C_{dc} = \frac{|I_S|}{4\xi\omega V_g} \tag{10}$$

Where the ripple factor is given by $\xi = V_{gpp}/V_g$. The parameters of DC filter capacitor C_{dc} computed from (8)-(10) for the proposed system are given in Table 2 for a 5% allowed ripple .

TABLE 2
PARAMETERS OF CAPACITOR C_{dc}

Capacitor value(mF)	16
Rated voltage (V)	500
Rated current, RMS (A)	14.4

The capacitor rated voltage is approximately equal to PV generator open circuit voltage. To prevent the DC-link capacitor from discharging through the PV generator under a failure in the interfacing inverter, a diode is inserted between the PV generator and DC-link capacitor, Fig. 1.

IV. CONTROL DESIGN

To facilitate the design of the controller, sufficiently high switching is assumed; therefore the grid line current could be considered nearly sinusoidal and in-phase with the grid voltage,

$$i_S = |I_S| \sin(\omega t) \tag{11}$$

Substituting (11) into (6)-(7) and ignoring the second harmonic components in the PV generator terminal voltage and inverter input current.

$$L_S |I_S| \cos(\omega t) + L_S \sin(\omega t) \frac{d|I_S|}{dt} = |V_g| \sin(\omega t) \cos(\delta) \tag{12}$$
$$+ |V_g| \cos(\omega t) \sin(\delta) - |V_S| \sin(\omega t) - R_S |I_S| \sin(\omega t)$$

$$C_{dc} \frac{dV_g}{dt} = I_g - \frac{|I_S|}{2} \cos(\delta) \tag{13}$$

Separating the coefficients of sin(ωt),

$$L_S \frac{d|I_S|}{dt} + |I_S| R_S = |V_g| \cos(\delta) - |V_S| \tag{14}$$

Considering a small disturbance around a steady-state operating point, the phase shift δ and the amplitudes of the PV generator terminal voltage V_g, current I_g and grid current $|I_S|$

are all perturbed but the grid voltage/frequency are assumed constant;

$$\delta=\delta_o+\Delta\delta \tag{15}$$

$$|I_S|=|I_{so}|+\Delta|I_S| \tag{16}$$

$$V_g=V_{go}+\Delta v_g \tag{17}$$

$$I_g=I_{go}+\Delta I_g \tag{18}$$

The variables with capital letters and 'o' as subscript represent steady-state components while the 'Δ ' prefix denotes a small-signal component of a variable. It is assumed that the small-signal components are several orders of magnitude less than the respective steady-state values. Substituting (16)-(18) into (4), (13) and (14) and multiplying out, neglecting products of small-signal terms, then applying Laplace Transform, the small-signal model of the system is given by,

$$sC_{dc}\Delta v_g=\Delta I_g-\frac{\Delta|I_S|}{2}\cos(\delta_o)+\frac{|I_{so}|}{2}\sin(\delta_o)\Delta\delta \tag{19}$$

$$sL_s\Delta|I_s|=\Delta v_g\cos(\delta_o)-V_{go}\sin(\delta_o)\Delta\delta-R_s\Delta|I_s| \tag{20}$$

$$\Delta v_g=-\frac{N_{ss}V_{th}}{M_{ss}I_{sc}}\left(\exp\left(-\frac{V_{go}-N_{ss}V_{oc}+\frac{N_{ss}I_{go}R_s}{M_{ss}}}{N_{ss}V_{th}}\right)+\frac{R_sI_{sc}}{N_{ss}V_{th}}\right)\Delta I_g=-k_g\Delta I_g \tag{21}$$

Solving (19)-(21), the open loop transfer function $\Delta I_g/\Delta V_g$ can be given by,

$$\frac{\Delta I_g}{\Delta\delta}=G_{g\delta}=-\frac{|I_{so}|\sin(\delta_o)(sL_s+R_s)+V_g\sin(\delta_o)\cos(\delta_o)}{s^2k_gC_{dc}L_s+2(L_s+k_gC_{dc}R_s)s+k_g\cos^2(\delta_o)+2R_s} \tag{22}$$

Equation (22) indicates that the transfer function $\Delta I_g/\Delta\delta$ is a second order; and it depends on the operating point of the system under concern. Moreover, the parameters of AC and DC filters dominate the shaping of the transfer function.

The frequency response of $\Delta I_g/\Delta\delta$ is shown in Fig. 4 for three different levels of solar irradiance: 200, 600 and 1000 Wm^{-2}. In developing Fig. 5 the temperature of the PV generator is kept constant at 25°C.

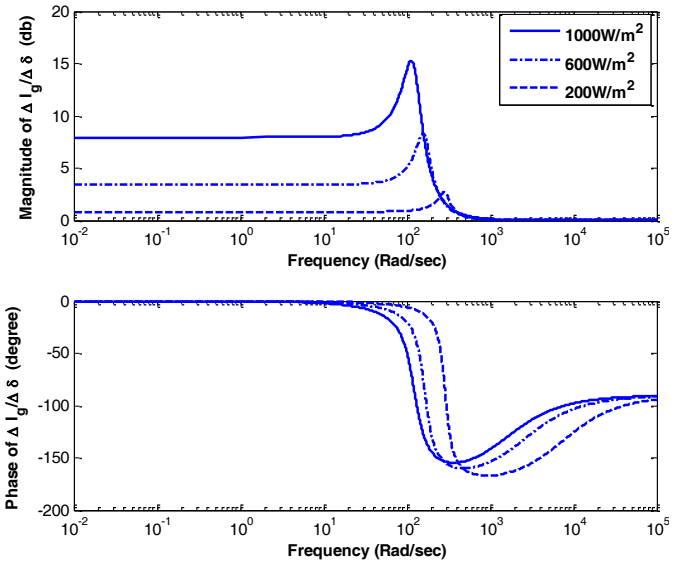

Fig. 5 Frequency response of $\Delta I_g/\Delta\delta$

The open loop frequency response of $G_{g\delta}$ is second order, and it has a pair of complex poles and a high frequency zero. The system, $G_{g\delta}$, has 8db gain at low frequency and slope of 40db/rad/sec at high frequency for 1000Wm^{-2} irradiance and 25°C temperature. The zero of $G_{g\delta}$ varies with the parameters of the AC side filter. The complex pole pair is dependent on PV generator power/current and parameters of DC and AC filters, and as shown from Fig. 5 the lowest natural frequency of the complex pole pair occurs at 1000Wm^{-2} and 25°C. Thus, the controller has to be tuned according to this operating point, which ensures satisfactory response at reduced levels of solar irradiance and PV generator power.

As previously mentioned, controlling the phase shift δ forces the PV generator to operate at maximum power point irrespective to irradiation levels. A PI controller is used for regulating the current I_g .The reference current is extracted by incremental conductance method. The parameters of the PI compensator are determined to maintain the system stability, offer adequate bandwidth under different operating conditions and provide sufficient attenuation for the low frequency ripples. The parameters of the PI compensator are given in Table 3 for the proposed system.

TABLE 3
PARAMETERS OF COMPENSATOR C_g

Proportional gain k_p	0.22
Integral gain k_i	0.0195

Using the controller C_g, Table 3, the frequency response of the closed loop transfer function $\Delta I_g/\Delta I_{ref}$ is given in Fig. 6.

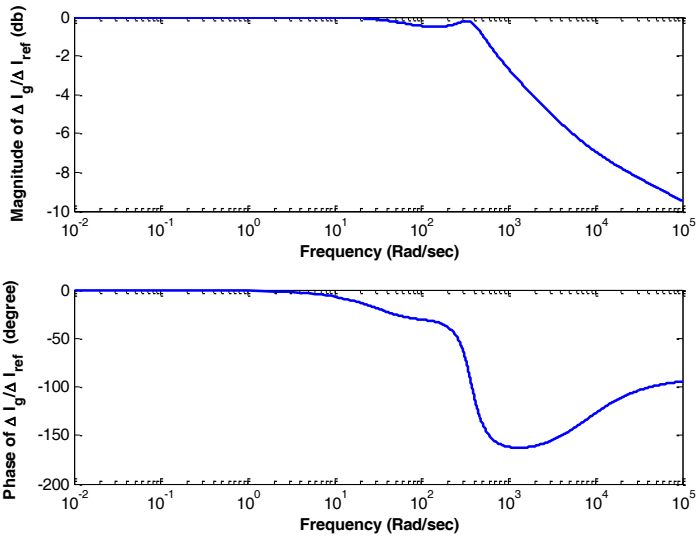

Fig. 6 Frequency response of closed loop transfer function $\Delta I_g/\Delta I_{ref}$

Fig. 6 shows that the controller in Table 3 resulted in bandwidth of around 180rad/sec. Increasing the bandwidth yields faster response, however, it results in significant ripple in the controlled signals, which deteriorates the grid current. Therefore the 180rad/sec bandwidth is considered a good comprise between the performance speed and the attenuation of the low frequency ripple in the feedback signals. It was found that the system bandwidth at reduced power levels is noticeably higher than, the design point, 180rad/sec. Therefore, the system is predicted to have faster response at reduced power levels.

V. RESULTS AND DISCUSSION

To validate the analysis, two programs in Micro-cap were developed; the first simulates the full detailed model, Fig. 1, while the second simulates the average model with the controller, Fig. 3. In the detailed model the power switching devices are assumed ideal. The detailed model utilizes three-level PWM modulation strategy at 10 kHz switching frequency. Therefore, the harmonics in the output voltage are centred on 20kz [17], and are attenuated by the AC side filter. The results from the programs of the average and full detailed models are compared in the following for different operating conditions. The parameters of the system, Fig. 1, used in the two programs are given in Table 4.

TABLE 4

Parameters of the proposed system, Fig. 1

Value of output filter inductance (mH)	5
Value of output filter resistance (Ω)	0.3
Grid voltage (RMS) (V)	220
Output frequency f_o (Hz)	60

In Figs. 7-10 solar irradiation is assumed to be available over 10 hours from 7 AM until 5 PM and vary almost sinusoidal; while its peak occurs at 12 AM. This represents an average day for the countries near equator as Egypt, particularly for rural and desert districts.

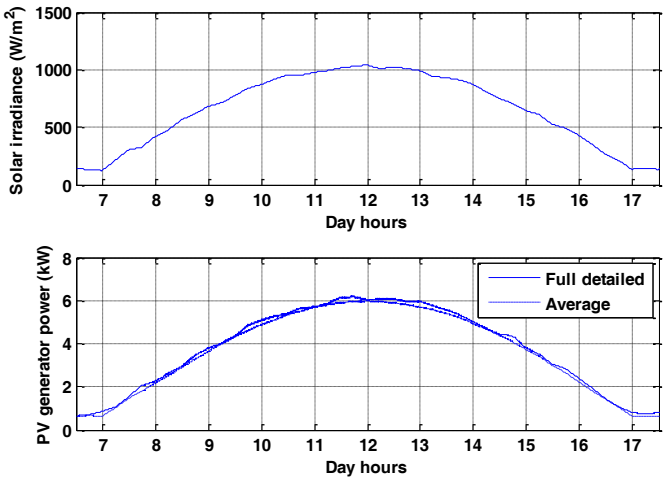

Fig. 7 Solar irradiance (top) and PV generator power (bottom) from average model (dashed) and detailed model (solid) for temperature of 25°C

Fig. 7 reveals the robustness of the controller and its ability of instantaneously tracking the MPP irrespective to operating point/solar irradiation level. A good agreement between the results from the detailed and average models is shown in Fig. 7. This demonstrates the validity of average model as simple, reliable and efficient tool in investigating the performance of single-phase PV grid-connected under different operating circumstances. Moreover, the simulation requirements regarding time and storage of the average model are significantly smaller compared with detailed model.

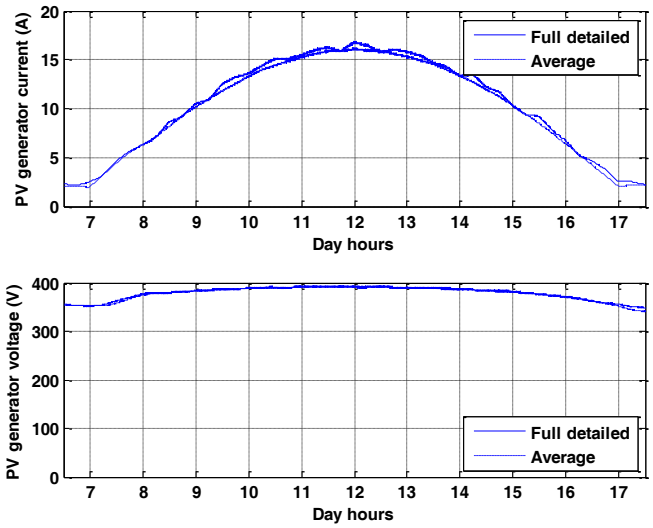

Fig. 8 PV generator current (top) and voltage (bottom) from average model (dashed) and detailed model (solid) for temperature of 25°C

The current of PV responds almost instantaneously to solar irradiation; on the contrary the PV voltage as shown in Fig. 7. This validates the conclusion extracted previously from Fig. 3. The PV voltage varies from 360V for 100W/m^2 solar irradiance to around 394V for 1000 W/m^2.

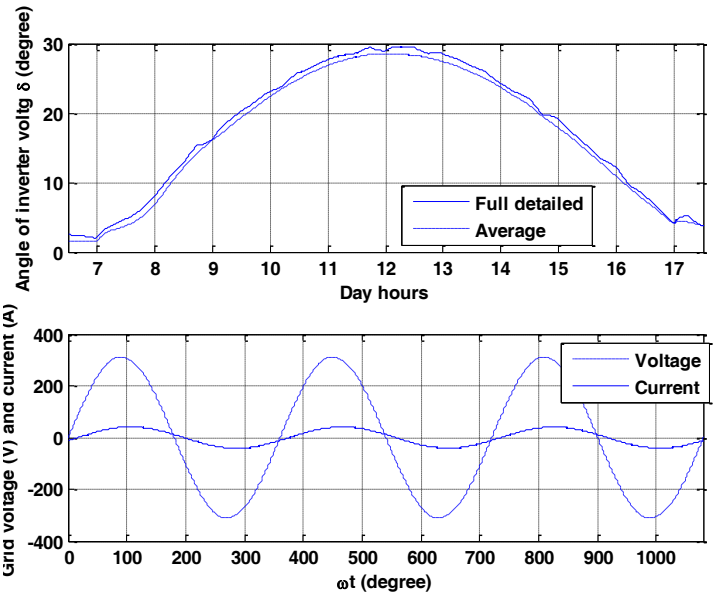

Fig. 9 Phase shift δ(top) from average model (dashed) and detailed model (solid) ; grid voltage (dashed) and current (solid) (bottom) for temperature of 25°C

Again a good agreement between the results of the switching model and the average model are shown in Fig. 9. The top graph in Fig.9 corroborates the relation between the phase shift δ and the current at MPP I_{MPP} that was identified in (2). The grid current is almost in phase with the grid voltage as shown in bottom graph, Fig. 9.

The bottom graph of Fig. 9 is drawn at peak of solar irradiance; however the phase shift between the grid voltage and current at other levels of solar irradiance was found not to exceed 10^{o}, which validated the assumption in (9). Moreover, the bottom graph in Fig. 8 shows that the grid current is almost sinusoidal.

Again Figs. 7-9 illustrate the adequacy of the controller in tracking MPP at different solar irradiance level.

The harmonic spectrum for the DC-link capacitor and grid currents are illustrated in Fig. 10 (a), at the peak of the solar irradiance, 1000Wm^{-2}, and 25°C temperature. The amplitudes of the harmonic components are plotted verus the harmonic order. In Fig. 10 (a), the harmonics are limited to 50^{th}, which corresponds to 3kHz; However, due to the switching strategy, there are harmonics in grid current and DC-link capacitor at multiples of switching frequency and its sidebands. For, the grid current the output inductor filter attenuates these harmonics effectively. However, for the DC link capacitor these harmonics should be carefully addressed, as the impedance of capacitor decreases inversely with the frequency. Fortunately, the amplitudes of these harmonics are much lower compared with the low frequency one.

The DC-link capacitor current obtained from the average model is shown in Fig. 10 (b). The current is plotted versus the time to show its frequency compared with that of the grid.

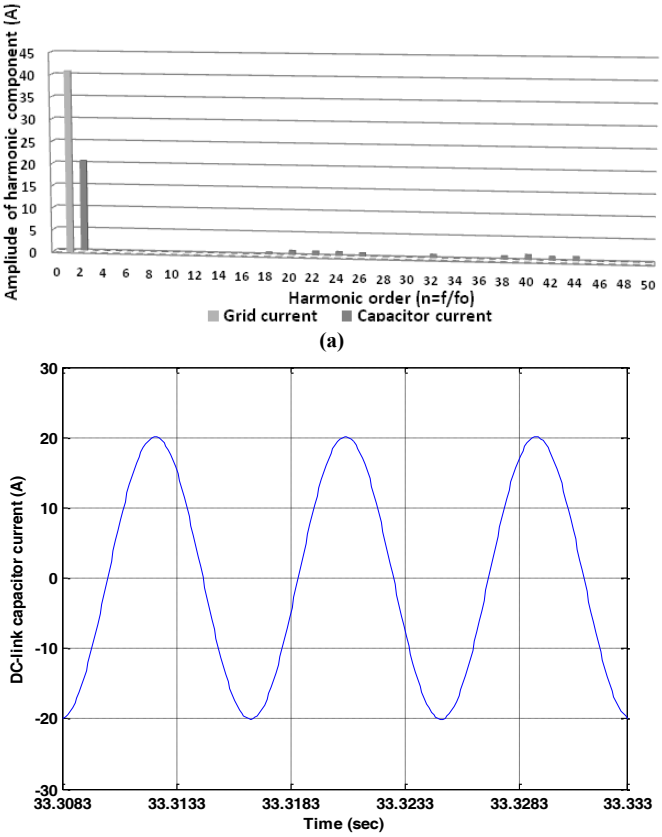

Fig. 10 DC-link capacitor current from average model and Harmonic spectrum for DC-link capacitor and grid currents at peak of the solar irradiance, 1000Wm^{-2}, and 25°C

(a) Harmonic spectrum for grid current (black)) and DC-link capacitor current (blue)

(b) DC-link capacitor current from average model

Fig. 10 shows that the DC-link capacitor current from average model corroborates with the full detailed models, which again expresses the significant of the average value model.

The Harmonic spectrum for the DC-link capacitor current, Fig.10, indicates that the low frequency ripple component is the severest, as it has the biggest amplitude, which mandates dimensioning the DC-link capacitor primarily to suppress this component, which correlates (10).

The modulation strategy used to synthesis the switching signals, has advantage of producing high quality grid current with THD less than 3%, Fig. 10.

VII. CONCLUSION

The following conclusions can be drawn:

- In single-phase grid-connected PV system, a significant ripple current component at twice the grid frequency flows in the DC-link. This mandates the application of large DC capacitor, otherwise this component circulates between the PV generator and the inverter, which reduces the system efficiency and the life cycle of the PV generator.
- An average value model of the single-phase grid-connected PV system was developed. The average model predicts the steady-state and dynamic performance of

system with reasonable accuracy as shown in the results. Moreover the average model requires less computation time and storage than the switching model. Therefore this model is considered as important tool in investigating the system performance under different operating conditions and in the designing of the controller.

- The voltage at MPP is considered to be less dependent on the solar irradiance.
- A simple PI controller was advised to allow the operation of the PV generator at MPP, while providing high quality grid current.
- A good correlation between the results from the average value and full detailed model was shown in the results.

REFERENCES

[1] J. T. Bialasiewicz "Power-Electronics Systems for the Grid Integration of Renewable Energy Sources : A Survey " IEEE Transactions on industrial Electronics, vol. 53, p. 1002:1016, August 2006-

[2] E. Endo and K. Kurokawa, "Sizing procedure for photovoltaic systems !in IEEE First World Conference on Photovoltaic Energy Conversion, 1994., , 1994, pp. 1196 - 1199-

[3] R. Geofrey; P. Walker and P. C. Serina, "Cascaded DC-DC Converter Connection of Photovoltiac Modules," *IEEE Transactions on Power Electronics*, vol. 19, pp. 1130-1139, 2004.

[4] A. K. S. Bhat, S. B. Dewan" DC-to-Utility Interface Using Sine Wave Resonant Inverter" IEE proceedings, vol. 135, part B, No. 5, September 1988, pp. 193-201.

[5] W. McMuarry, " Modulation of the chopping frequency in DC choppers and PWM inverters having current hysteresis controllers" IEEE Transaction Industry application, vol. IA-20, July/August 1984, pp. 763-768.

[6] Y. Zhao; Y. Zhang; D. Wang and J. Zhan " The Circuit Topology for Single-phase Grid-connected System and the Control Technology on Converters" International Conference on Sustainable Power Generation and Supply, 2009. SUPERGEN '09 ,6-7 April 2009 +pp. 240-249

[7] E. Roman, R. Alonso, P. Ibanez, S. Elorduizapatarietxe, D. Goitia, "Intelligent PV Module for Grid-Connected PV Systems," IEEE Transactions on industrial Electronics, vol. 53, pp. 1066-1073 +June 2006-

[8] W. Yi-Bo;, W. Chun-Sheng;, L. Hua;, X. Hong-Hua;, and Page(s):, "Steady-state model and power flow analysis of grid-connected photovoltaic power system !in IEEE International Conference on Industrial Technology, 2008. ICIT 2008, pp. 1 - 6.

[9] D. Casadei, G. Grandi, and Claudio Rossi " Single-Phase Single-Stage Photovoltaic Generation System Based on a Ripple Correlation Control Maximum Power Point Tracking" !IEEE Transactions on Energy Conversion, vol. 21, pp. 562-568, June 2006.

[10] A. D. Theocharis, A. Menti, J. Milias-Argitis and Th. Zacharias" Modeling and Simulation of a Single-phase Residential Photovoltaic System".

[11] T. Esram, P. L. Chapman " Comparison of Photovoltiac Array Maximum Power Point Tracking Techniques" IEEE Transactions on Energy Conversion, vol. 22, 2007.

[12] S. Yuvarajan, S. Xu" Photovoltaic power converter with a simple maximum-power-point-tracker " Proceeding of 2003 *International Symposium on Circuit and Systems* 2003, pp. III-399-III-402

[13] J. H. Lee; H. Bae and B. H. Cho "Advanced Incremental Conductance MPPT Algorithm with a Variable Step Size" Proceeding of EPE-Power Electronics and Machines Conference 2006, pp. 603-607.

[14] A. A. hafez, "simple and robust Maximum Power Point Tracking Algorithm for solar cell," in World Congress on Electronics and Electrical Engineering (WCEEENG'10), Luxor. Egypt, 4-8April 2010-

[15] Kyocera, http://www.kyocerasolar.com/products/pdf/specsheets/kd_210gx-lp_081508, March, 2010.

[16] M. G. Villalva; J. R. Gazoli and E. R. Filho," Comprehensive Approach to Modeling and Simulation of Photovoltaic Arrays" IEEE Transaction on Power Electronics, vol. 24, pp. 1198-1208, MAY 2009.

[17] N. Mohan, T. M. Undeland, and W. P. Robbins, "*Power Electronics: Converters, Applications, and Design"*, 2nd edition. New York, Chichester, Wiley, 1995.